

Development of a Classical Force Field for the Oxidised Si Surface: Application to Hydrophilic Wafer Bonding

Daniel J. Cole* and Mike C. Payne

*Theory of Condensed Matter Group, Cavendish Laboratory,
University of Cambridge, J J Thomson Avenue, Cambridge, CB3 0HE, UK*

Gábor Csányi

*Centre for Micromechanics, Department of Engineering,
University of Cambridge, Trumpington Street, Cambridge, CB2 1PZ, UK*

S. Mark Spearing

*Engineering Materials Group, School of Engineering Sciences,
University of Southampton, Southampton, SO17 1BJ, UK*

L. Colombi Ciacchi

*Fraunhofer Institut für Werkstoffmechanik
Wöhlerstrasse 11, 79108 Freiburg, Germany and
Institut für Zuverlässigkeit von Bauteilen und Systemen,
University of Karlsruhe, Kaiserstr. 12, 76131 Karlsruhe, Germany.*

(Dated: October 22, 2018)

Abstract

We have developed a classical two- and three-body interaction potential to simulate the hydroxylated, natively oxidised Si surface in contact with water solutions, based on the combination and extension of the Stillinger-Weber potential and of a potential originally developed to simulate SiO₂ polymorphs. The potential parameters are chosen to reproduce the structure, charge distribution, tensile surface stress and interactions with single water molecules of a natively oxidised Si surface model previously obtained by means of accurate density functional theory simulations. We have applied the potential to the case of hydrophilic silicon wafer bonding at room temperature, revealing maximum room temperature work of adhesion values for natively oxidised and amorphous silica surfaces of 97 mJ/m² and 90 mJ/m², respectively, at a water adsorption coverage of approximately 1 monolayer. The difference arises from the stronger interaction of the natively oxidised surface with liquid water, resulting in a higher heat of immersion (203 mJ/m² vs. 166 mJ/m²), and may be explained in terms of the more pronounced water structuring close to the surface in alternating layers of larger and smaller density with respect to the liquid bulk. The computed force-displacement bonding curves may be a useful input for cohesive zone models where both the topographic details of the surfaces and the dependence of the attractive force on the initial surface separation and wetting can be taken into account.

I. INTRODUCTION

Direct wafer bonding has emerged as an important technology for silicon-based microelectronic and micromechanical systems.^{1,2} In particular, the preparation of silicon-on-insulator devices takes advantage of the strong adhesion between oxidised and hydrated Si surfaces to bond together crystalline Si wafers without the need for adhesives or high pressures.^{3,4} The first step of the bonding process is the preparation of hydrophilic Si surfaces, in which a ~ 0.5 nm thin layer of native oxide covers the Si bulk and is terminated by chemisorbed hydroxyl groups and hydrogen-bonded water molecules. Afterwards, the surfaces are put in contact at room temperature by applying a small pressure in a localised region of the wafers. This triggers the propagation of a bonding front to the whole surface area,⁵ in a process that is driven by the formation of a hydrogen-bonded water network trapped between the Si surfaces.¹ Finally, the bonded system is annealed at high temperature to induce condensation of adjacent silanols on opposite surfaces and diffusion of trapped water molecules away from the interface, forming a SiO₂ layer between the Si wafers.

Crucial for the formation of a defect-free bonded interface is complete bonding during the room temperature contacting step. To this end, the prepared surfaces need to be sufficiently flat and clean and the non-covalent interactions between them sufficiently strong. The experimental evidence points towards a dependence of the interaction strength on the amount of water physisorbed on the surfaces,⁶ which is approximately 1 monolayer (ML) at a relative humidity of about 70 %.⁷ Moreover, under similar humidity conditions, the adhesion strength depends substantially on the details of the oxide structure covering the surfaces. The measured work of adhesion for natively oxidised surfaces with 1-2 ML of adsorbed water is approximately 100 mJ/m².⁸ In the case of thicker oxide layers, obtained after thermal oxidation of the Si surface, lower values in the range 60-85 mJ/m² have been reported.⁹ These are consistent with the bonding energy associated with the closure of cracks in vitreous silica glass.⁶ Here the measured work of adhesion is about 75 mJ/m² for relative humidities above 20 %, but is found to rapidly decrease at lower humidity. Notably, equal adhesion strengths could be measured in experiments of crack opening or closing,⁶ pointing towards a reversible adhesion mechanism governed by hydrogen bonds and ruling out the formation of covalent bonds between the surfaces at room temperature. This is supported by a molecular dynamics simulation of amorphous silica wafers, which suggests a water-mediated adhesion

mechanism in the absence of siloxane bridges across the bonding interface.¹⁰

In this work, we perform classical molecular dynamics (MD) simulations to investigate the crucial role of trapped water during the room temperature stage of hydrophilic Si wafer bonding. In particular, we aim to investigate surfaces terminated by a native oxide layer, whose structure and composition have been previously determined by means of extensive first principles molecular dynamics (FPMD) simulations based on density functional theory.^{11,12} For this purpose, we develop a classical force field capable of reproducing the interactions between all chemical species present in the Si/SiO_x/water interface system previously obtained by FPMD. Our starting points are the well-known Stillinger-Weber potential,¹³ which has been widely used to simulate Si bulk crystal structures, and a potential developed by Vashishta and co-workers to study the structure and energetics of SiO₂ polymorphs.¹⁴ Here we combine these two potentials, extending them to take into account the full range of Si oxidation states present in the native oxide layer as well as the interactions between the oxide layer and liquid water.

After describing the details of the potential development (Section II) and the technical details of the MD simulations (Section III), our investigation will start with the study of the structural and energetic details of the interfaces of both amorphous silica and natively oxidised Si with liquid water (Section IV A). Subsequently, results of our investigation into the hydrophilic bonding of pairs of silica wafers and natively oxidised Si wafers will be reported and compared (Section IV B). Finally, all of our main findings will be briefly discussed and summarised in Section V.

II. FORCE FIELD DEVELOPMENT

A. Reference model structure

Under normal atmospheric conditions, the Si surface is passivated by a hydroxylated native oxide layer less than 1 nm in thickness. In Ref. 11, the oxidation of the Si(001) surface in a dry environment has been investigated by means of FPMD simulations based on density functional theory (DFT). In good agreement with medium-energy ion scattering experiments,¹⁵ it was found that oxygen spontaneously adsorbs onto the bare surface up to a coverage of 1.5 ML. At higher coverages, further oxide growth becomes limited by diffusion

of O_2 molecules to the reactive Si/SiO_x interface. In a subsequent work, water molecules were found to spontaneously adsorb and dissociate on the resulting oxide structure, creating further reactive sites for reactions with oxygen molecules.¹² The oxidised and partially hydrated surface structure obtained in this series of FPMD simulations after the adsorption of seven oxygen and two water molecules is shown in Fig. 1. The resulting concentration of 4 hydroxyl groups on a 1.2 nm² surface is consistent with values ranging between 2.6 and 4.6 OH/nm² measured experimentally on amorphous silica surfaces.^{16,17} The 13 oxidised Si atoms in the final structure present variable formal valence charges ranging from Si⁺ to Si⁴⁺, in ratios which are roughly consistent with the available experimental literature.¹⁵ We have performed a Mulliken population analysis of this structure (projecting the ground state wave functions onto a basis consisting of s and p atomic orbitals) and found that the charges on the Si atoms increase approximately linearly with the number of nearest-neighbour O atoms, which act as electron acceptors (Table I).

We have shown, in a recent work, that surface oxidation in a dry environment is accompanied by the development of tensile surface stress up to 2.9 N/m at a coverage of 1.5 ML.¹⁸ The surface stress g is defined as the basis invariant trace of the stress tensor σ multiplied by half the height a of the periodically repeated supercell:¹⁹

$$g = \frac{1}{2}a \text{Tr}(\sigma_{\alpha\beta}) = \frac{1}{2}a(\sigma_{yy} + \sigma_{zz}),$$

From the above equation, using the same DFT technique as in Ref. 18 (see Ref. 20), we have calculated the surface stress present in the relaxed hydroxylated native oxide, obtaining a value of 2.5 N/m (after subtracting the surface stress of the bottom hydrogen-terminated surface). This value is slightly lower than for the dry oxidised structure, since the dissociative adsorption of water on the native oxide has broken strained Si–O bonds, although the surface clearly remains under tensile stress.

B. Potential form for the natively oxidised Si surface

We turn now to the development of a charge-based classical potential, whose analytic form and parameters will be constructed so as to reproduce the structure and tensile stress of the *ab initio* reference model described above. Our starting points are the well-known Stillinger-Weber potential¹³ (SW), which has been widely used to simulate bulk properties of

silicon, and a potential developed by Vashishta et al. to simulate bulk and surface properties of silica polymorphs^{14,21} (VP). Both of these potential energy functions contain only two- and three-body particle interactions and may be expressed by the general form:

$$V = \sum_{1 \leq i < j} V_{ij}(\mathbf{r}_{ij}) + \sum_{1 \leq i < j < k} V_{ijk}(\mathbf{r}_{ij}, \mathbf{r}_{ik}, \mathbf{r}_{jk}),$$

where the indices i and j run over all atoms of the simulated system and \mathbf{r}_{ij} is the vector connecting atom i with atom j . Our aim here is to combine the SW and VP potentials into a single form and extend them to include the full range of Si oxidation states present in the native oxide layer. In order to ensure that our potential reduces to the original forms^{13,14} in the limits of bulk Si and bulk SiO₂, cut-off functions to the two- and three-body interactions will be introduced to smoothly interpolate between potential regimes. The form of these cut-off functions will be chosen so as to ensure that the potential energy and the forces on the particles are continuous functions of the particles' coordinates. This is essential to account for possible breaking and forming of Si–O bonds in MD simulations of the surface with our potential form.

In the VP potential, atomic charges with values of $+1.6 e^-$ and $-0.8 e^-$ are assigned to the Si⁴⁺ and O²⁻ species, respectively.¹⁴ To maintain the original potential form in the case of Si⁴⁺ species, we assign to the oxidised Si atoms and to the O atoms quantised partial charges according to:

$$q_{Si} = +0.4 \sum_O f_c(r, R_q, \Delta_q)$$

$$q_O = -0.4 \sum_{Si} f_c(r, R_q, \Delta_q).$$

According to the expression above, in agreement with the trend in computed Mulliken charges (see Table I), the charges on the oxidised Si species increase linearly with the number of oxygen neighbours up to a value of $+1.6$ for fully oxidised Si⁴⁺ species. The number of atomic neighbours is defined by the cut-off function f_c , which falls off smoothly and with continuous derivative over a distance interval 2Δ around a cut-off distance R :

$$f_c(r, R, \Delta) = \begin{cases} 1, & r < R - \Delta \\ 1 - \frac{r-R+\Delta}{2\Delta} + \frac{\sin[\pi(r-R+\Delta)/\Delta]}{2\pi}, & R - \Delta \leq r < R + \Delta \\ 0, & r \geq R + \Delta. \end{cases}$$

As anticipated above, the Si–Si two-body interactions are as in the SW potential, with the addition of a Coulomb term arising from the possible presence of charges on the Si atoms:

$$V_{Si-Si'} = A(q_{Si}, q_{Si'})[Br^{-4} - 1]\exp(\sigma(r - a)^{-1})f_c(r, R_{Si}, \Delta_{Si}) + \frac{q_{Si}q_{Si'}}{r}.$$

In the *ab initio* reference structure, the Si–Si bond lengths are observed to be approximately independent of the Si oxidation state. Therefore, in an adjustment to the original expression,¹³ the SW parameter A in the equation above includes a charge dependence, which counteracts the Coulomb repulsion between oxidised Si atoms (Fig. 2):

$$A(q, q') = A_0(1 + 3.2qq')f_A(q)f_A(q').$$

Si⁴⁺ species, as found in the tetrahedral form of SiO₂, form no direct Si–Si bonds and are instead connected via bridging oxygen atoms. Hence, the factor $f_A(q)$ is used here to remove the Si–Si attraction for Si⁴⁺ species, recovering the purely repulsive behaviour of the original VP potential:

$$f_A(q) = \begin{cases} 1.0 & q \leq 1.2 \\ 4.0 - 2.5q & 1.2 < q < 1.6 \\ 0.0 & q \geq 1.6. \end{cases}$$

The form of the Si–O two-body interaction is based on Ref. 14 and is made up of three terms: a short range steric repulsion, a charge-dipole attraction and a Coulomb attraction:

$$V_{Si-O} = \left(\frac{C_{SiO}(q_{Si})}{r^9} - \frac{D_{SiO}}{r^4}\exp(-r/b) \right) f_B(q_{Si}) + \frac{q_{Si}q_O}{r};$$

$$C_{SiO}(q) = C_0 - C_1q;$$

$$f_B(q) = \begin{cases} 2.5q & q \leq 0.4 \\ 1.0 & q > 0.4. \end{cases}$$

In the *ab initio* reference structure, the Si–O bond lengths decrease approximately linearly with increasing oxidation state of Si. By varying the hard-core repulsion parameter C_{SiO} as a function of charge, we aim to reproduce the increase in bond length for oxidised Si atoms other than Si⁴⁺ (Fig. 3). The cut-off function $f_B(q)$ is introduced to reduce the uncharged, sub-surface Si atoms' interactions with O atoms in the oxide layer in order to recover the pure SW potential form within the Si bulk.

The O–O interaction is exactly as in Ref. 14 and contains the same contributions as the Si–O interaction:

$$V_{O-O'} = \frac{C_{OO'}}{r^7} - \frac{D_{OO'}}{r^4} \exp(-r/b) + \frac{q_O q_{O'}}{r}.$$

The three-body interactions are all of the same SW form with parameters adapted from the literature,^{13,14,22} again smoothed by cut-off functions f_c to recover the original VP potential:

$$V_{ijk} = \lambda \exp[\gamma_1(r_{ij} - d_1)^{-1} + \gamma_2(r_{ik} - d_2)^{-1}] (\cos\theta_{jik} - \cos\theta_0)^2 f_c(r_{ij}, R_{Si}, \Delta_{Si}) f_c(r_{ik}, R_{Si}, \Delta_{Si}).$$

Finally, the hydroxyl groups that terminate the oxide surface are assigned charges equal to:

$$q_O = -0.4 \sum_{Si} f_c(r, R_q, \Delta_q) - 0.2$$

$$q_H = +0.2,$$

consistent with the charge of approximately -0.6 assigned to the oxygen atoms of terminal silanol groups on the quartz surface in Ref. 23. The O–H bond length is constrained to 0.975 \AA and the Si–O–H interaction takes the above three-body form, with the parameters chosen to reproduce the variation about the minimum energy of the Si–O–H three-body interaction of Ref. 23.

It should be emphasised that the potential form described here reduces exactly to the original SW and VP potentials for bulk Si and SiO₂ under equilibrium conditions. The cut-off distance R_{Si} is chosen to ensure that two- and three-body interactions involving Si are switched on when Si–Si separations are in the region of 2.6 to 2.8 \AA or below. In bulk Si (equilibrium bond length 2.36 \AA), our potential reproduces the SW potential up to bond lengths of 2.6 \AA , after which the attraction is smoothly reduced to zero, as shown by the dashed curve in Fig. 2. Similarly, our potential may be applied to SiO₂ polymorphs (Si–Si nearest neighbour peak separation of 3.1 \AA in amorphous silica, for example), reducing exactly to the VP potential for Si–Si separations greater than 2.8 \AA (apart from an additional Si–Si hard-core repulsion present in the original VP form, which is negligible for separations above 1 \AA). Below this Si–Si separation, we introduce repulsive Si–Si–O and Si–Si–Si three-body interactions, while the Si–Si two-body interaction is removed entirely by the cut-off function $f_A(q)$.

Starting from the original values of the parameters for the separate SW and VP potentials,^{13,14} the values of all parameters used in our two- and three-body interactions have been

carefully adjusted to reproduce as accurately as possible the *ab initio* reference structure in Fig. 1, and are listed in Table II. Average bond lengths and angles after minimisation of the hydroxylated surface structure, using this parameter set, show reasonable agreement with the *ab initio* minimised structure (Table III). The calculated surface stress with our potential parameters is 2.0 N/m, consistent with the *ab initio* computed tensile stress of 2.5 N/m. Importantly, no change in the topology of the SiO_x network (i.e. no breaking or forming of Si–O bonds) was observed during 50 ps of classical MD simulation at 300 K, during which the charges and potential parameters were updated at every time step.

As an additional test of our potential, we have performed a dynamical simulation of a Si/SiO₂ interface system composed of a 11 Å thick slab of Si and a 17 Å thick slab of α -quartz. At the interface, the Si(001) surface has been matched with the SiO₂ surface by expanding the α -quartz lattice parameter by 10 % in one direction to form an ideal, defect-free heterojunction. The system was separately annealed for 100 ps at 500 K, 100 ps at 700 K and for 50 ps at 1000 K. In none of these systems was breaking of existing bonds or formation of new bonds observed. Moreover, the average Si–O bond lengths and Si–O–Si angles at the interface have been found to decrease from their bulk values by about 1 % and 4 % respectively, in agreement with a number of previous investigations.^{24,25} This demonstrates a certain degree of transferability of our potential to study Si/SiO_x heterogeneous systems. As a note of caution, we must say that we do not necessarily expect our potential to be predictive as far as the formation of unknown structures during chemical reactions (such as oxidation processes) is concerned. However, this may become possible upon augmentation of the potential within hybrid quantum/classical schemes such as the recently developed “Learn on the Fly” technique.²⁶

C. Interactions between the oxidised surface and water

To study the behaviour of SiO_x surfaces in a wet environment, we model the interactions between the surface atoms and water molecules as a sum of Coulomb (via atomic partial charges) and Van der Waals (VdW) contributions. Consistent with force fields used to simulate solvated biomolecules in solution, the VdW interactions between water molecules and the surface hydroxyl groups are described by a “hydrogen bond” form $V(r_{ij}) = A/r_{ij}^{12} - B/r_{ij}^{10}$, with the A and B parameters taken from standard AMBER parameter sets.²⁷ The

VdW interactions between water molecules and all other atom types are of the standard Lennard-Jones (LJ) form:

$$V(r_{ij}) = 4\epsilon_{ij} \left(\left(\frac{\sigma_{ij}}{r_{ij}} \right)^{12} - \left(\frac{\sigma_{ij}}{r_{ij}} \right)^6 \right) .$$

For each pair of atoms we define: $\epsilon_{ij} = \sqrt{\epsilon_i \epsilon_j}$ and $\sigma_{ij} = 2^{-1/6}(\sigma_i + \sigma_j)$, such that the minimum energy separation, r_0 , is $\sigma_i + \sigma_j$, and $V(r_0) = -\sqrt{\epsilon_i \epsilon_j}$.

It has to be noted that the values of the partial charges on the surface atoms have been chosen so as to guarantee stability of the SiO_x network (see previous section). In particular, their values differ from the atomic point charges which best fit the electrostatic potential in a region outside the VdW radius of the atoms (ESP charges), which would be the best choice of charges to simulate the surface hydration properties.²⁸ For this reason, we have adapted the parameters of the LJ part of the non-bonded surface-water potential so as to reproduce the binding energy curves for isolated water molecules on selected surface sites obtained in *ab initio* calculations. This energy is mostly accounted for by electrostatic effects, which are well described within standard DFT techniques.

Within DFT,²⁰ we have calculated the total energy of a single water molecule as a function of its distance from the hydroxylated surface for two configurations, chosen such that the main interactions present are between one H atom of water with an O atom of the surface and between the O atom of water with a Si^{4+} atom of the surface (Fig. 4). Identical total energy calculations were performed using the TIP3P water model²⁹ and our newly developed force field for the native oxide, for different choices of the LJ parameters of the water-surface interactions. The best obtained binding energy curves are shown in Fig. 4, and the corresponding, optimised set of LJ parameters is reported in Table IV. As will be shown in Section IV A, with this set of parameters the calculated heat of immersion of an amorphous silica surface amounts to 166 mJ/m^2 , which should be compared with the experimental value of 158 mJ/m^2 , measured for a surface with a density of terminal $-\text{OH}$ groups of 3.4 nm^{-2} .³⁰

III. COMPUTATIONAL DETAILS

All classical simulations were performed using the DLPOLY.3 MD package,³¹ in which our newly-developed force field for the native oxide could be easily implemented. Long-

ranged Coulomb interactions were treated using the Ewald sum, with a real space cut-off of 8 Å. Newton’s equations of motion were integrated with the velocity Verlet algorithm and a time step of 1 fs, using the RATTLE algorithm³² to constrain O–H bond lengths. Where necessary, temperature control was achieved by velocity rescaling.

An amorphous silica model was generated according to existing MD schemes,³³ using the VP potential in its original form,¹⁴ which has been successfully applied to study amorphous silica surfaces.²¹ Namely, we initially placed 1314 randomly positioned Si and O atoms, in the ratio 1 : 2, in a periodically repeated $30 \times 30 \times 20$ Å³ simulation cell. The initial structure was annealed for 100 ps at 8000 K, then for a further 100 ps at 4000 K. Subsequently, the system was cooled to 300 K over a period of 360 ps, switching to a constant pressure ensemble controlled by a Nosé-Hoover combined thermostat and barostat with 0.2 ps relaxation times. Following a further 200 ps annealing at 300 K, the bulk density was 2.37 g/cm³ (compared to the experimental value of 2.20 g/cm³).¹⁴ Further structural analysis, detailed in Fig. 5 and Table V, was in good agreement with the literature¹⁴ and revealed the presence of a network of corner-sharing SiO₂ tetrahedra.

Starting from the bulk amorphous silica structure obtained, a 50 Å vacuum layer was inserted in the z -direction of the simulation cell, resulting in separated, periodically repeated slabs of surface area 9.1 nm². The resulting surfaces were annealed at 1000 K for 500 ps, cooled to 300 K over 750 ps and, finally, annealed at 300 K for a further 500 ps, all at constant volume. These long annealing times were necessary to stabilise the concentrations of defects, found here in the form of threefold coordinated Si atoms and dangling O atoms, with converged concentrations of 1.6 nm⁻² and 1.7 nm⁻², respectively. These concentrations may be compared to Ref. 34, which uses a Born-Mayer-Huggins pair interaction and a similar three-body potential, obtaining concentrations of the two defect types of 0.6 nm⁻² and 1.9 nm⁻². Fig. 6, left, reveals that these defects were located in the first 5 Å of the surface. In agreement with an existing VP potential simulation of the amorphous silica surface,²¹ we found that the surface was terminated by dangling O atoms and that surface O–Si–O bond angles were shifted to higher angles, indicating the presence of under-coordinated Si, as shown in Fig. 6, right. After terminating these two defect types with –OH and –H groups, respectively, and relaxing the whole system, the resulting hydroxylated amorphous silica surface had a hydroxyl group surface concentration of 3.3 nm⁻², which lies in the range of experimental measurements (2.6 - 4.6 nm⁻²).^{16,17}

To model the hydroxylated native oxide on Si(001), the *ab initio* reference structure shown in Fig. 1 was periodically repeated in the surface plane to form a 3×3 slab of surface area 10.6 nm^2 . The bottom surface was terminated with a copy of the oxide layer after rotation through 180° and translation by a bulk Si lattice parameter. The resulting slab consisted of 792 Si atoms, corresponding to eleven layers, oxidised and hydroxylated on either side with a total of 288 O and 72 H atoms. The lattice parameter was fixed to the equilibrium value for bulk Si obtained with the SW potential (5.44 \AA), and the vacuum gap in the direction perpendicular to the surface plane was set to 50 \AA , as in the case of the amorphous silica slab.

To investigate water layering at the two hydroxylated surfaces (Section IV A), the 50 \AA vacuum layers were filled with TIP3P water molecules²⁹ at a density of approximately 1 g/cm^3 . For each surface, the entire system was equilibrated at 300 K and the height of the supercell adjusted to remove the stress in the direction perpendicular to the surface. Particle coordinates were collected every 100 time steps over a 1 ns production run. Selected snapshots from these simulations were used to construct the initial input files for the simulations of hydrophilic wafer bonding (Section IV B), keeping in the simulation cells only the water molecules closest to the surfaces up to heights corresponding to the desired surface water coverages. Based on the structural analysis of the surface/water interfaces (Section IV A), one ML of adsorbed water is found to contain 98 and 117 water molecules on the amorphous silica and native oxide surface models, respectively, which correspond to surface densities of 10.7 and 11.0 molecules/ nm^2 .

Based on Ref. 10, force-displacement curves were calculated by reducing the height of the simulation cell perpendicular to the surfaces (and thus the separation between the top surface and the periodic image of the bottom surface) at a rate of 0.1 \AA every 11 ps. At each separation distance, the system was first equilibrated and thermalised to 300 K by velocity rescaling for 1 ps. During the subsequent 10 ps, the particle coordinates were collected every 0.2 ps and the average z component of the stress in the simulation cell was calculated. In this way, the net interfacial force could be computed as a function of separation distance and the resulting curve integrated to obtain the total surface bonding energy.

IV. RESULTS AND DISCUSSION

A. Structure and energetics of the $\text{SiO}_x/\text{Water}$ interface

We start our investigation of the interactions between wet oxidised silicon surfaces by studying the structure of bulk water in contact with both the amorphous silica and the natively oxidised Si surfaces. Any surface in contact with bulk water will have an effect on the intrinsic ordering of water in its proximity. In particular, water molecules will interact strongly with and partly penetrate into hydrophilic surfaces to form surface-water hydrogen bonds, in competition with water-water hydrogen bonds in the liquid. This will result in a layered structure of water molecules close to the surface, which can be quantified by the surface density profile of water molecules along the direction perpendicular to the surface.

We have calculated the density profiles of water in contact with the two surface models by computing the average number of water molecules present in 0.1 \AA thin, planar slices parallel to the surface during a 1 ns simulation, as described in Section III. The results are reported in Fig. 7. In each case, we found evident structuring of water in layers of higher and lower density with respect to the bulk, consistent with previous simulations of a hydrophilic quartz surface.²³ For both surfaces, the position of the main peak in the density profile matches the position of the outermost surface hydroxyl group. The presence of subsidiary peaks closer to the surface, especially in the case of natively oxidised Si, is indicative of water penetration into the relatively open structure of the hydroxylated surfaces, as expected. With respect to the position of the first maximum (of density 1.05 g/cm^3), the water density close to the amorphous silica surface presents a trough at a distance of 1.1 \AA and a second maximum at 2.3 \AA , before reaching the bulk water density of 0.98 g/cm^3 at a distance of approximately 4 \AA . The main peak at the native oxide surface is higher, reaching 1.32 g/cm^3 , and the oscillations continue out to approximately 5 \AA from the position of the main peak before reaching the bulk water density.

The shape of the density profile obtained allows us to define a ML as the layer of water molecules contained between the surface and the position of the first trough after the main density peak. By integration of the density profiles, 98 and 117 water molecules are found to be contained in 1 ML on the amorphous silica and the natively oxidised surfaces, corresponding to surface densities of 10.7 and 11.0 water molecules/ nm^2 , or to surface areas per

water molecule of 9.3 and 9.1 Å², respectively. These values should be compared with early assumptions,⁷ where an area of 10.6 Å² has been assigned to a water molecule adsorbed on quartz, the difference arising probably from the number of molecules which are able to penetrate relatively deeply into the surface oxide structures.

For each surface, we have computed the heat of immersion as the difference between the energy of the system in contact with water and the energies of the two separate components, namely the dry surface model and bulk water. For each immersed system, the energy has been computed as the average value of the potential energy obtained in separate MD simulations at 300 K for 1 ns. With this approach, we calculated heat of immersion values of 166 mJ/m² and 203 mJ/m² for the amorphous silica and native oxide respectively. The first of the two values may be compared with experimentally measured values of 157 mJ/m² or 158 mJ/m², for surfaces with estimated densities of terminal –OH groups of 2.3 nm⁻² or 3.4 nm⁻².^{30,35} The excellent agreement between the experimental and the theoretical values provides good support for the parametrisation of our surface-water potential, as described in Section II C. We note that a possible deprotonation of the surface hydroxyl groups in the experimental system is not expected to influence substantially the results obtained. In fact, in deionised water at pH 7, the surface charge is expected to be of the order of -1 μC/cm²,³⁶ corresponding to just one deprotonated hydroxyl group per simulation cell, which is unlikely to contribute significantly to the computed heat of immersion.

A further insight into the details of the surface/water interfaces may be gained by analysing the average number of surface-water and water-water hydrogen bonds formed per water molecule within the first ML compared with the liquid bulk. Considering a hydrogen bond to be present between two O atoms when the O–H···O angle is greater than 140° and the O–O separation is smaller than 3.5 Å, the calculated average number of hydrogen bonds per molecule in bulk water is 3.13. Close to the surface, within the first ML, the corresponding values for the amorphous silica and the native oxide are 3.30 and 3.27, respectively, reflecting the competitive hydrogen bond formation at the surface. In each case, 0.76 hydrogen bonds per molecule are formed with the surface (Table VI), which can be further divided between the bonds donated to O atoms bridging Si atoms of the surface, the bonds donated to O atoms of terminal hydroxyl groups, and the bonds received by H atoms of hydroxyl groups. The calculated values (Table VI) indicate evident differences between the two surfaces. Namely, more hydrogen bonds are formed between water and bridging

oxygen atoms in the case of the native oxide structure, probably due to the reduced charge on some of the Si atoms, and thus the reduced electrostatic screening, compared with the amorphous silica surface. Since the charges on the bridging oxygen atoms are higher than those on the hydroxyl groups, this may help to explain the difference between the computed heat of immersion in the two cases, despite the small difference in the number of water molecules per surface area within the first ML.

B. Wafer Bonding

In the previous subsection, we have shown how competitive hydrogen bond formation at the surface/water interface leads to a local restructuring of the hydrogen bond network between the molecules. This results in oscillations in the water density, which propagate several Angstroms into the bulk liquid. The thin layer of water trapped between oxidised silicon wafers in the room temperature stage of hydrophilic wafer bonding will be subjected to the same effect, whose relationship to the attractive force between the wafers will be investigated below.

We have calculated the average net force present between two bare amorphous silica surfaces and two bare native oxide surfaces in the absence of any water molecules as a function of the interface separation according to the procedure described in Section III. Starting from two separated surfaces, no attraction is observed when the surfaces are moved together (dashed lines in Fig. 8, top). When the surfaces become very close to each other, steric repulsion occurs between the surface atoms and the repulsive force increases rapidly. Zero separation in the curves in Fig. 8 was defined as the point of onset of this repulsive force.

The situation is very different in the presence of water molecules between the surfaces. In Fig. 8, top, we have plotted the force-separation curves calculated at increasing water coverages (from approximately 0.25 to 2.5 ML per surface), along with the associated hydrogen bond density as a function of surface separation (Fig. 8, bottom). As the surfaces move together, they experience a net attractive force (negative values in the reported plots), which initially increases, reaches a maximum value and then decreases, becoming repulsive at small separations. Subsequent debonding simulations, in which the surfaces were pulled apart at the same rate, revealed no hysteresis in the force-separation curves.

The overall behaviour of the system may be rationalised by looking at the number of hydrogen bonds formed per molecule between the surfaces. Starting from larger separations, the hydrogen bond density increases as the surfaces come into closer and closer contact. At smaller separations, if the concentration of water is smaller than about 1 ML (dotted lines in Fig. 8), the interaction between the surfaces becomes repulsive well before the hydrogen bond density reaches the equilibrium values of 3.30 or 3.27 at the amorphous silica or native oxide surfaces, respectively (see Section IV A). In these cases, the computed force becomes dominated by the repulsion between the two solid surfaces, and the repulsive part of the force-separation curve tends to that calculated in the absence of trapped water. On the other hand, for water coverages greater than approximately 1 ML (solid lines in Fig. 8), the onset of repulsion occurs before the surfaces interact directly. In fact, as is visible in Fig. 8, the point of zero force between the surfaces at increasing water coverages tends to the point at which the density of hydrogen bonds reaches 3.13, the equilibrium value in bulk water.

These results imply that there is an optimum water concentration for room temperature hydrophilic wafer bonding, low enough that there is a high concentration of energetically favourable surface-water hydrogen bonds, as observed within the first ML of the systems in Section IV A, but high enough that the oxide surface repulsion does not dominate. By integration of the force-displacement curves we can compute the energy gained during the simulated bonding process, that is the work of adhesion of the wet surfaces Q_{ad} . This is reported as a function of the water coverage in Fig. 9, indeed showing an optimum water concentration for bonding at approximately 1 ML for both surface models. At very low coverages, the steric repulsion between the surface dominates, so that Q_{ad} rapidly decreases to negligible values. At the other extreme, for high coverages, the values of Q_{ad} are very similar in the two cases and tend to the value of bulk TIP3P water, calculated by integration of a force-separation curve for a water-water interface, in the absence of any solid surface. The value obtained, 78 mJ/m², is indicated with a dotted line in Fig. 9 and may be compared with the experimental surface energy of 72 mJ/m² for the water-air interface at room temperature.³⁷

For the case of amorphous silica, the variation of Q_{ad} with water coverage may be compared with forces associated with crack closure in vitreous silica glass at different relative humidities, as reported in Ref. 6. In this comparison, we shall take into account that Q_{ad} is half the strain energy release rate, and that each value of relative humidity is associated

with a well-defined coverage of adsorbed water.⁷ The investigation in Ref. 6 shows that, at high humidity, Q_{ad} is roughly constant at about 75 mJ/m², which corresponds to the surface energy of bulk water. At relative humidities lower than about 20 %, which corresponds to a water coverage of approximately 0.5 ML, Q_{ad} starts to decrease and drops to 25 mJ/m² at a coverage of approximately 0.25 ML. This is in good agreement with the shape of the amorphous silica curve shown in Fig. 9, where the computed work of adhesion is 19 mJ/m² at 0.25 ML coverage, and is comparable with the surface energy of bulk water at large coverages. In our simulations, Q_{ad} presents a small peak of 90 mJ/m² at approximately 1 ML. Experimental values of work of adhesion in direct surface bonding experiments using silica glasses are lower, in the range of 60 to 85 mJ/m²,⁹ which might be explained by the microroughness present in the experimental wafer samples.³⁸

As far as the natively oxidised Si surface is concerned, our simulations indicate a slightly higher maximum value of Q_{ad} than amorphous silica, which may be related to the higher heat of immersion and to the more pronounced oscillations of the density close to the surface, as reported in Fig. 7. In fact, the water density profiles between closely spaced native oxide surfaces show oscillations that match those observed at an isolated slab (Fig. 10). At 0.5 ML coverage, the main peaks from opposite surfaces overlap, producing a single peak in the water density at equilibrium (Fig. 10, top right), fully consistent with trapping 1 ML of water between the two surfaces. In this case, as shown in Fig. 10, top left, the initial force required to separate the surface and thus break the hydrogen bond network of this ML is high, although Q_{ad} is relatively low, due to the surface-surface repulsion at small separation. At 1.0 ML coverage, Q_{ad} is maximum, reaching 97 mJ/m², in good agreement with experimental values of approximately 100 mJ/m² for natively oxidised Si wafers covered by 1-2 ML of water.⁸ In this case, the main peaks in the equilibrium water density at the two surfaces are separated by 2.5 Å (Fig. 10, bottom left), close to the ideal O–O separation of 2.8 Å for hydrogen-bonded TIP3P water.²⁹ This indicates the existence of an ordered, energetically stable, hydrogen-bonded water network, spanning the two bonded wafers. Finally, at higher coverages, the density in the central region between the wafer is constant, roughly at the equilibrium density of bulk water (Fig. 10, bottom right), consistent with Q_{ad} being comparable with the surface energy of liquid water.

In an ideal debonding experiment, Q_{ad} may be thought of as being composed of a large energy loss (positive values) associated with breaking the network of hydrogen bonds between

the wafers and with an energy gain associated with the rearrangement of water at the surfaces, to optimise the number of hydrogen bonds per molecule. The more structured the water layer, the smaller will be the energy gain, due to the reduced capability of water to rearrange within the layer (which is consistent with the measured lower entropy of water molecules at low coverages on oxidised surfaces⁷). Therefore, the slightly larger Q_{ad} value than in the case of amorphous silica may be explained by the more pronounced structuring of water between the native oxide surfaces induced by the stronger surface-water interactions (see Section IV A).

V. SUMMARY AND CONCLUSIONS

In conclusion, we have developed a force field which enables us to investigate, at the classical level, the interactions between oxidised Si surfaces and a liquid environment. This is of particular importance given the increasingly wider fields of application of silicon-based microelectromechanical devices put in direct contact with water solution, such as sensors or actuators used in a physiological environment.³⁹ In our potential form, the surface interacts with the external environment through non-bonded interactions of the electrostatic and Van der Waals type, which makes the combination of the developed potential with standard force fields used to investigate biological macromolecules straightforward, and opens the way to large-scale simulations of biomolecule adsorption on realistic Si surfaces models. Moreover, the form of our force field allows processes associated with a rearrangement of the Si–O bond network to be simulated, as is necessary for the application of classical Hamiltonians in hybrid quantum-classical schemes of the “Learn on the Fly” type.²⁶ These appear to be very promising tools for the atomistic simulations of chemo-mechanical effects (for example, those occurring at a crack tip during a stress-corrosion process), which require both large system sizes and accurate quantum description of limited portions of the simulated systems.^{40,41,42}

In this work, we have applied the newly developed potential to the simpler case of hydrophilic Si wafer bonding at room temperature, where no breaking or forming of covalent bonds is expected to play a role. We have found that our parameterisation of the interatomic potential is able to reproduce the structural and mechanical properties of the natively oxidised Si surface, as obtained in previous FPMD simulations based on DFT.^{11,12} Moreover, calculated energetic details of the amorphous silica/water interface, such as the surface heat

of immersion, were found to agree well with existing experimental measurements. As compared with the amorphous silica surface, the natively oxidised Si surface was found to interact more strongly with the liquid water, resulting in a higher heat of immersion (203 mJ/m^2 vs. 166 mJ/m^2) and a more pronounced structuring of the water molecules close to the surface in alternating layers of larger and smaller density with respect to the liquid bulk.

The layering of water at the oxidised surface has a profound effect on the computed force-displacement curves in simulated wafer bonding experiments at different coverages of adsorbed water. We have predicted that there is an optimum surface water concentration for bonding between both glassy silica and natively oxidised Si surfaces, for which the maximum work of adhesion values are 90 mJ/m^2 and 97 mJ/m^2 , respectively, occurring at approximately 1 ML coverage (corresponding to about 70 % relative humidity⁷). It must be noted that these values refer to perfectly flat surfaces, whereas experimentally measured values are expected to depend heavily on the nanoscale surface roughness present in the samples.³⁸ This is especially true in the case of bonding experiments, where a work of adhesion as low as 40 mJ/m^2 has been measured for two natively oxidised Si surfaces.⁵ The relatively slow diffusion of water parallel to the surface will prevent a perfect wetting of the whole surface during bonding. However, in subsequent fracture tests the work of adhesion has been shown to rise to 120 mJ/m^2 , possibly due to rearrangement of the water layer over the length scale of the surface roughness.⁴³ Our calculated force-displacement curves may provide a useful input for macroscopic models where both the topographic details of the bonded surfaces and the precise dependence of the attractive force on the initial surface separation and wetting can be taken into account. Combining the results presented here with these macroscopic models, such as the cohesive zone model of Kubair and Spearing,⁴⁴ will be the subject of future work.⁴⁵

Acknowledgements

We would like to thank Yohsataka Umeno for useful discussions and suggestions. Computational resources were provided by the Cambridge HPC Service, U.K., by the Zentrum für Informationsdienste und Hochleistungsrechnen, Dresden, and by the HLRS Stuttgart within the AQUOXSIM project and through the HPC-Europa project (RII3-CT-2003-506079, with the support of the European Community - Research Infrastructure Action of the FP6). LCC

acknowledges support by the Alexander von Humboldt Stiftung, by the Japanese Society for the Promotion of Science and by the Deutschen Forschungsgemeinschaft within the Emmy Noether Programme. This work has been supported by the EPSRC, U.K.

- * Electronic address: djc56@cam.ac.uk
- ¹ Q. Y. Tong and U. Gösele, *Semiconductor Wafer Bonding: Science and Technology* (Wiley, New York, 1998).
- ² M. Reiche, *Phys. Stat. Sol. (a)* **203**, 747 (2006).
- ³ J. B. Lasky, *Appl. Phys. Lett.* **48**, 78 (1986).
- ⁴ M. Shimbo, K. Furukawa, K. Fukuda, and K. Tanzawa, *J. Appl. Phys.* **60**, 2987 (1986).
- ⁵ K. T. Turner and S. M. Spearing, *Proc. R. Soc. A* **462**, 171 (2006).
- ⁶ T. A. Michalske and E. R. Fuller, *J. Am. Ceram. Soc.* **68**, 586 (1985).
- ⁷ J. W. Whalen, *J. Phys. Chem.* **65**, 1676 (1961).
- ⁸ Q. Y. Tong and U. Gösele, *Annu. Rev. Mater. Sci.* **28**, 215 (1998).
- ⁹ W. P. Maszara, G. Goetz, A. Caviglia, and J. B. McKitterick, *J. Appl. Phys.* **64**, 4943 (1988).
- ¹⁰ D. A. Litton and S. H. Garofalini, *J. Appl. Phys.* **89**, 6013 (2001).
- ¹¹ L. Colombi Ciacchi and M. C. Payne, *Phys. Rev. Lett.* **95**, 196101 (2005).
- ¹² L. Colombi Ciacchi, J. Bagdahn, D. J. Cole, M. C. Payne, and P. Gumbsch, Stress-driven Oxidation Chemistry of Wet Silicon Surfaces, submitted for publication.
- ¹³ F. H. Stillinger and T. A. Weber, *Phys. Rev. B* **31**, 5262 (1985).
- ¹⁴ P. Vashishta, R. K. Kalia, and J. P. Rino, *Phys. Rev. B* **41**, 12197 (1990).
- ¹⁵ Y. Hoshino, T. Nishimura, T. Nakada, H. Namba, and Y. Kido, *Surf. Sci.* **488**, 249 (2001).
- ¹⁶ A. S. D'Souza and C. G. Pantano, *J. Am. Ceram. Soc.* **82**, 1289 (1999).
- ¹⁷ L. T. Zhuravlev, *Colloids and Surfaces A: Physiochem. Eng. Aspects* **173**, 1 (2000).
- ¹⁸ D. J. Cole, M. C. Payne, and L. Colombi Ciacchi (2007), Stress Development and Impurity Segregation during Oxidation of the Si(100) Surface, *Surf. Sci.*, to be published.
- ¹⁹ D. Vanderbilt, *Phys. Rev. Lett.* **59**, 1456 (1987).
- ²⁰ Our calculations are performed within the spin-polarised density functional theory using the PBE gradient-corrected exchange correlation functional and ultrasoft pseudopotentials. The wave functions are expanded in plane waves up to a kinetic energy cutoff of 400 eV and a Gaus-

sian smearing function of width 0.01 eV is applied to the electronic occupancies. Calculations on the hydroxylated native oxide surface are performed using a periodically repeated slab of 8 Si layers with 8 atoms per layer, sampling the Brillouin zone with two \mathbf{k} -points at $(0, \pm 0.25, 0.25)$. The surface slab is terminated on the top surface by the hydroxylated native oxide layer and on the bottom surface by 8 H atoms and separated from its periodic image in the x -direction by a vacuum layer equivalent to 8 Si layers. The lattice parameters parallel to the surface are fixed to the calculated Si bulk equilibrium value of 5.454 Å.

- ²¹ M. I. Trioni, A. Bongiorno, and L. Colombo, *J. Non. Cryst. Sol.* **220**, 164 (1997).
- ²² T. Watanabe, H. Fujiwara, H. Noguchi, T. Hoshino, and I. Ohdomari, *Jpn. J. Appl. Phys.* **38**, L366 (1999).
- ²³ P. E. M. Lopes, V. Murashov, M. Tazi, E. Demchuk, and A. D. MacKerell Jr., *J. Phys. Chem. B* **110**, 2782 (2006).
- ²⁴ A. A. Demkov and O. F. Sankey, *Phys. Rev. Lett.* **83**, 2038 (1999).
- ²⁵ T. Watanabe, K. Tatsumura, and I. Ohdomari, *Appl. Surf. Sci.* **237**, 125 (2004).
- ²⁶ G. Csányi, T. Albaret, M. C. Payne, and A. De Vita, *Phys. Rev. Lett.* **93**, 175503 (2004).
- ²⁷ D. A. Pearlman, D. A. Case, J. W. Caldwell, W. R. Ross, T. E. Cheatham, S. DeBolt, D. Ferguson, G. Seibel, and P. Kollman, *Comp. Phys. Commun.* **91**, 1 (1995).
- ²⁸ C. I. Bayly, P. Cieplak, W. D. Cornell, and P. A. Kollman, *J. Phys. Chem.* **97**, 10269 (1993).
- ²⁹ W. L. Jorgensen, J. Chandrasekhar, J. D. Madura, R. W. Impey, and M. L. Klein, *J. Chem. Phys.* **79**, 926 (1983).
- ³⁰ T. Takei, E. Eriguchi, M. Fuji, T. Watanabe, and M. Chikazawa, *Thermochimica Acta* **308**, 139 (1998).
- ³¹ I. Todorov and W. Smith, *Phil. Trans. R. Soc. Lond. A* **362**, 1835 (2004).
- ³² H. C. Andersen, *J. Comput. Phys.* **52**, 24 (1983).
- ³³ B. P. Feuston and S. H. Garofalini, *J. Appl. Phys.* **68**, 4830 (1990).
- ³⁴ B. P. Feuston and S. H. Garofalini, *J. Chem. Phys.* **91**, 564 (1989).
- ³⁵ T. Takei and M. Chikazawa, *J. Colloid Interface Sci.* **208**, 570 (1998).
- ³⁶ G. H. Bolt, *J. Phys. Chem.* **61**, 1166 (1957).
- ³⁷ W. V. Kayser, *J. Coll. Interface Sci.* **56**, 622 (1976).
- ³⁸ N. Miki and S. M. Spearing, *J. Appl. Phys.* **94**, 6800 (2003).
- ³⁹ A. C. Richards Grayson, R. S. Shawgo, A. M. Johnson, N. T. Flynn, Y. Li, M. J. Cima, and

- R. Langer, Proceedings of the IEEE **92**, 6 (2004).
- ⁴⁰ J. R. Kermode, T. Albaret, D. Sherman, N. Bernstein, P. Gumbsch, M. C. Payne, G. Csányi, and A. De Vita, Low Speed Instabilities of Crack Propagation in Silicon, submitted for publication.
- ⁴¹ G. Moras, L. Colombi Ciacchi, G. Csányi, and A. De Vita (2007), (100) Hydrogen-induced Platelets in Silicon: a Multiscale Molecular Dynamics Approach, Physica B, to be published.
- ⁴² B. Q. Luan, S. Hyun, J. F. Molinari, N. Bernstein, and M. O. Robbins, Phys. Rev. E **74**, 046710 (2006).
- ⁴³ K. T. Turner and S. M. Spearing (2007), Accurate Characterization of Wafer Bond Toughness with the Double Cantilever Specimen, Appl. Phys. Lett., to be published.
- ⁴⁴ D. V. Kubair and S. M. Spearing, J. Phys. D: Appl. Phys. **40**, 3070 (2007).
- ⁴⁵ D. V. Kubair, D. J. Cole, L. Colombi Ciacchi, and S. M. Spearing, Multiscale Mechanics Modeling of Direct Silicon Wafer Bonding, to be submitted.

Tables

TABLE I: Distribution of Mulliken charges in the reference structure of an oxidised and hydrated Si surface obtained in a series of FPMD simulations. Charges are multiples of the electronic charge.

Species	Mulliken Charges	Average
Si ⁺	0.62 0.65 0.46 0.47 0.61	0.56
Si ²⁺	1.26 1.28 1.28	1.27
Si ³⁺	1.79 1.82 1.79	1.80
Si ⁴⁺	2.30 2.34	2.32

TABLE II: Parameters of the interatomic potential. Units of length are Å and those of energy are e²/Å(= 14.39 eV).

Two-body potential parameters

R_q	2.0	A_0	1.062	C_0	14.871	$C_{OO'}$	51.692
Δ_q	0.1	B	11.603	C_1	2.178	$D_{OO'}$	1.536
R_{Si}	2.7	a	3.771	b	4.43		
Δ_{Si}	0.1	σ	2.0951	D_{SiO}	3.072		

Three-body potential parameters

λ_{SiSiSi}	3.164	λ_{SiSiO}	3.164	λ_{SiOSi}	1.400	λ_{OSiO}	0.350	λ_{SiOH}	0.521
$\gamma_{1,SiSiSi}$	2.51	$\gamma_{1,SiSiO}$	4.06	$\gamma_{1,SiOSi}$	1.00	$\gamma_{1,OSiO}$	1.00	$\gamma_{1,SiOH}$	1.00
$\gamma_{2,SiSiSi}$	2.51	$\gamma_{2,SiSiO}$	0.52	$\gamma_{2,SiOSi}$	1.00	$\gamma_{2,OSiO}$	1.00	$\gamma_{2,SiOH}$	1.00
$d_{1,SiSiSi}$	3.771	$d_{1,SiSiO}$	3.981	$d_{1,SiOSi}$	2.60	$d_{1,OSiO}$	2.60	$d_{1,SiOH}$	2.60
$d_{2,SiSiSi}$	3.771	$d_{2,SiSiO}$	2.933	$d_{2,SiOSi}$	2.60	$d_{2,OSiO}$	2.60	$d_{2,SiOH}$	2.60
$\theta_{0,SiSiSi}$	109.47°	$\theta_{0,SiSiO}$	109.47°	$\theta_{0,SiOSi}$	141.00°	$\theta_{0,OSiO}$	109.47°	$\theta_{0,SiOH}$	122.50°

TABLE III: Comparison between *ab initio* and classical minimisations of the hydroxylated Si(001) surface. In the *ab initio* structure, Si–O bond lengths (Å) increase with decreasing Si oxidation state, while Si–Si bond lengths remain approximately constant. In the classical simulation, although some bond lengths and angles have changed, there is no restructuring of the surface. Si–O–H angles (126°) also agree with DFT values (127°).

	<i>ab initio</i> structure					classical structure				
	Si-O	Si-Si	O-Si-O	Si-Si-O	Si-Si-Si	Si-O	Si-Si	O-Si-O	Si-Si-O	Si-Si-Si
Si ⁴⁺	1.64	–	109°	–	–	1.63	–	109°	–	–
Si ³⁺	1.65	2.36	109°	109°	–	1.61	2.41	119°	96°	–
Si ²⁺	1.67	2.39	109°	108°	109°	1.62	2.44	139°	101°	110°
Si ⁺	1.70	2.38	–	108°	111°	1.65	2.39	–	108°	111°

TABLE IV: LJ parameters optimised for the surface-water interactions. Water OW parameters are taken from the TIP3P water model. Parameters for water HW atoms are for interactions with Si and OB only, otherwise ϵ_i is zero. In the surface, OB refers to bridging O atoms and OH to hydroxyl O atoms.

	water		surface			
	OW	HW	Si	OB	OH	H
$\epsilon_i/\text{eV}\times 10^{-2}$	0.66	0.13	1.30	1.13	0.65	0.09
$\sigma_i/\text{Å}$	1.768	0.650	1.600	1.762	1.650	1.000

TABLE V: MD results for amorphous silica at 300K. The peak bond length or angle and the corresponding full width at half maximum (FWHM) of each distribution is reported and compared to Ref. 14.

	this work		Ref. 14	
	bond length/Å	FWHM/Å	bond length/Å	FWHM/Å
Si-O	1.62	0.07	1.62	0.05
O-O	2.63	0.20	2.64	0.15
Si-Si	3.09	0.27	3.10	0.20
	bond angle	FWHM	bond angle	FWHM
O-Si-O	108°	12°	109.6°	10°
Si-O-Si	141°	26°	142.0°	25°

TABLE VI: Statistics of hydrogen-bonding between the two surfaces and the first ML of water (within the first peak of the density distribution).

Surface	OW-HW...OW	OW-HW...OB	OW-HW...OH	OH-H...OW	Total surface
a-SiO ₂	2.54	0.14	0.30	0.32	0.76
native	2.51	0.24	0.26	0.26	0.76
bulk water	3.13	-	-	-	-

Figure Captions

FIG. 1: Side and top views of the hydroxylated native oxide layer on Si(001) as obtained in a series of FPMD simulations.^{11,12} O atoms (red) either bridge two Si atoms or form part of a terminating hydroxyl group. The valence states of the 13 oxidised Si atoms range from Si^+ to Si^{4+} .

FIG. 2: Examples of the Si-Si two-body interaction for Si^{0+} - Si^{0+} species (dashed line) and Si^{2+} - Si^{1+} species (dotted line), compared with the original SW interaction for uncharged Si (solid line). The equilibrium bond lengths are similar and both potentials tend to the Coulomb interaction for large separations.

FIG. 3: The Si-O two-body interaction. The equilibrium bond length increases with decreasing Si partial charge.

FIG. 4: DFT (dashed lines) and classical (solid lines) binding energy curves of a single water molecule above the hydroxylated native oxide surface. In each simulation, the water molecule is displaced vertically, and the relative total energy is plotted as a function of its separation, d , from the surface. In the first configuration (left, black curves), the water molecule, with a H atom pointing downwards is bound to a bridging O atom. In the second configuration (right, blue curves), the water O atom is pointing downwards towards a Si atom and is repelled from the surface.

FIG. 5: (left) Total radial distribution function in bulk amorphous silica. The first three peaks correspond to Si-O, O-O and Si-Si nearest neighbours. (right) O-Si-O and Si-O-Si bond angle distributions, which are consistent with a network of corner-sharing SiO_2 tetrahedra.

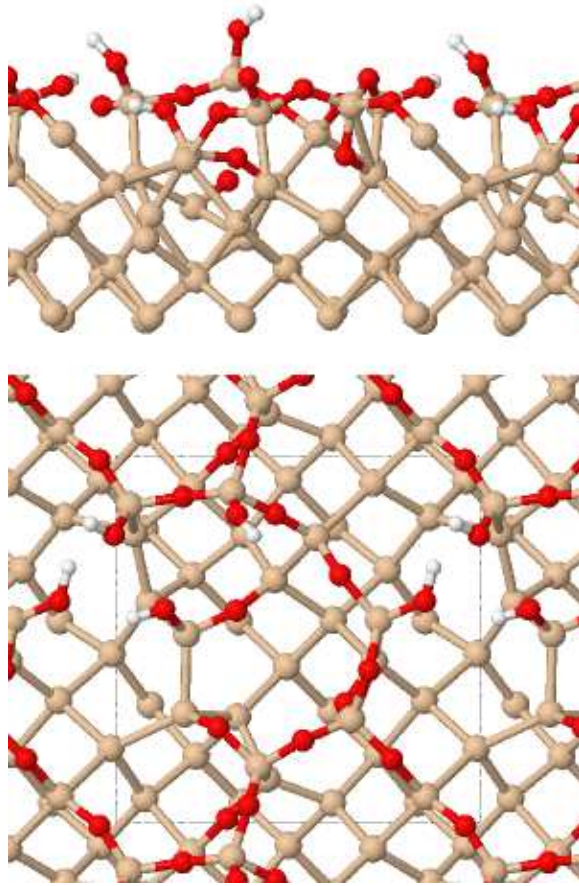
FIG. 6: (left) Relative densities of fourfold coordinated (Si-4) and threefold coordinated (Si-3) Si atoms and bridging (O-2) and dangling (O-1) O atoms with increasing distance from the centre of the amorphous silica slab. Defects are concentrated in the first 5 Å of the surface. (right) O–Si–O bond angles near the surface (dashed line) show broadening out to larger angles than in the bulk (solid line), indicating the presence of Si-3 species.

FIG. 7: Average density of water molecules perpendicular to the hydroxylated amorphous silica (left) and native oxide (right) surfaces. In both cases, the main peak is centred on the surface/water interface, with some water penetrating the surfaces and density oscillations continuing into the water layer. The water density in the centre of the simulation cells matches that of bulk water.

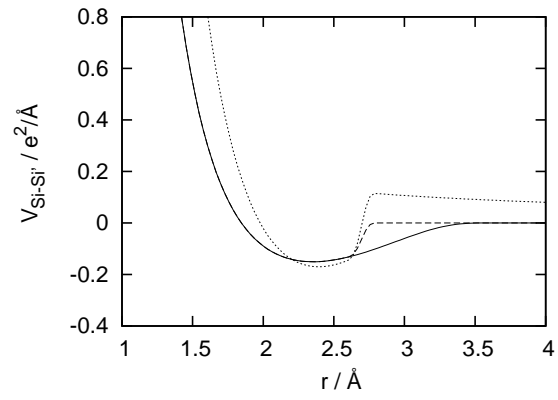
FIG. 8: (top) Force-separation curves for two hydroxylated amorphous silica (left) and native oxide (right) surfaces. The bare surfaces (dashed lines) repel (positive force) at separations below 0 Å. Also plotted, from left to right, are curves corresponding to approximately 0.25, 0.50, 0.75, 1.00, 1.50, 2.00 and 2.50 ML water coverage on each surface. The curves are translated upwards so that the force, at large separations, is zero. (bottom) Number of hydrogen bonds per water molecule as a function of surface separation for the amorphous silica (left) and native oxide (right) surfaces. Below about 1 ML (dotted lines), the number of hydrogen bonds does not reach the ideal surface density (upper dashed lines) before the surfaces repel. The maximum attractive force between surfaces at higher water coverages (solid lines) is limited by the hydrogen bond density between the surfaces, which tends to that of bulk water (lower dashed lines).

FIG. 9: Surface energy of two hydroxylated amorphous silica (solid line) and native oxide (dashed line) surfaces as a function of water coverage. The bonding energy of silica is approximately constant, with a small peak at 1 ML, and decreases at low coverages. The native oxide surfaces are more strongly bound at low coverages, before tending to the silica and bulk water surface energies at high coverages.

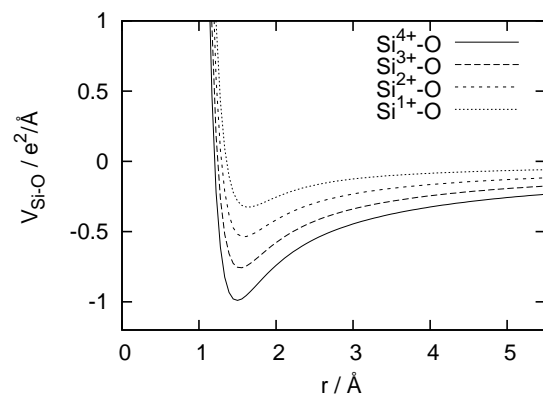
FIG. 10: Average water density profiles perpendicular to two natively oxidised Si wafers at equilibrium separation, at increasing water coverage. The corresponding force-separation curves are numbered (top left). At 0.5 ML coverage (1), a large force is required to separate the single density peak into two. At 1.0 ML (2), the bonding energy is a maximum, because a stable water network is set up between the two wafers. At 2.5 ML (3), the interfacial water density and associated surface energy is close to that of bulk water.



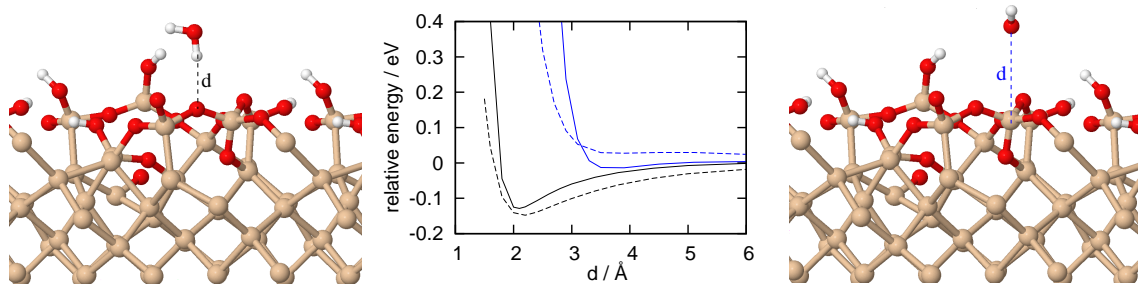
D. J. Cole et al., Figure 1



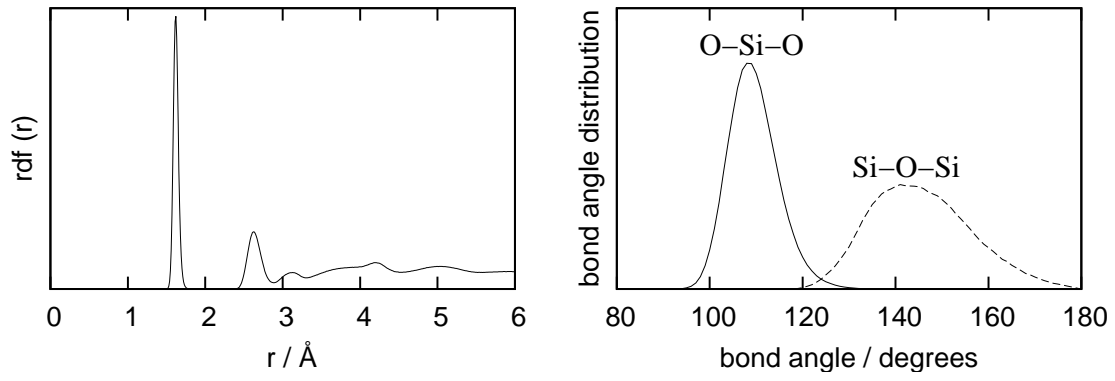
D. J. Cole et al., Figure 2



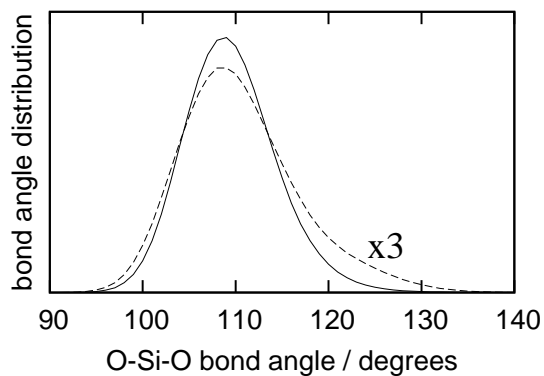
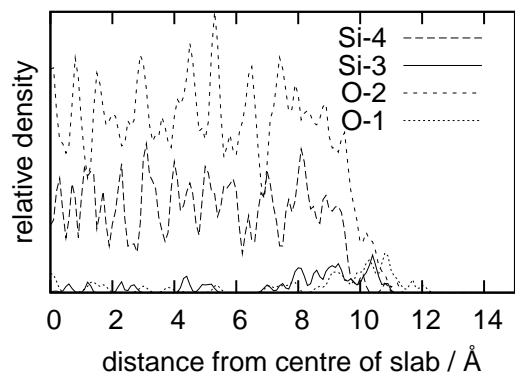
D. J. Cole et al., Figure 3



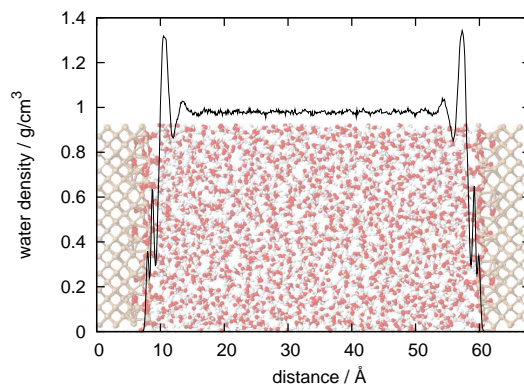
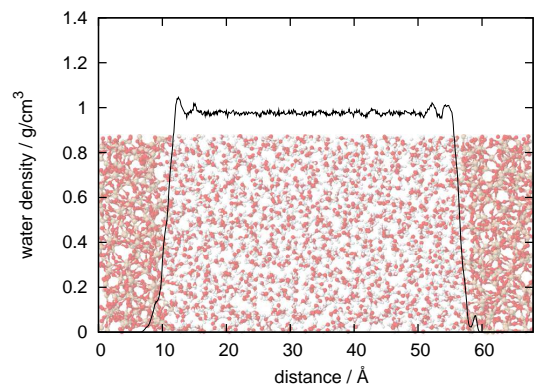
D. J. Cole et al., Figure 4



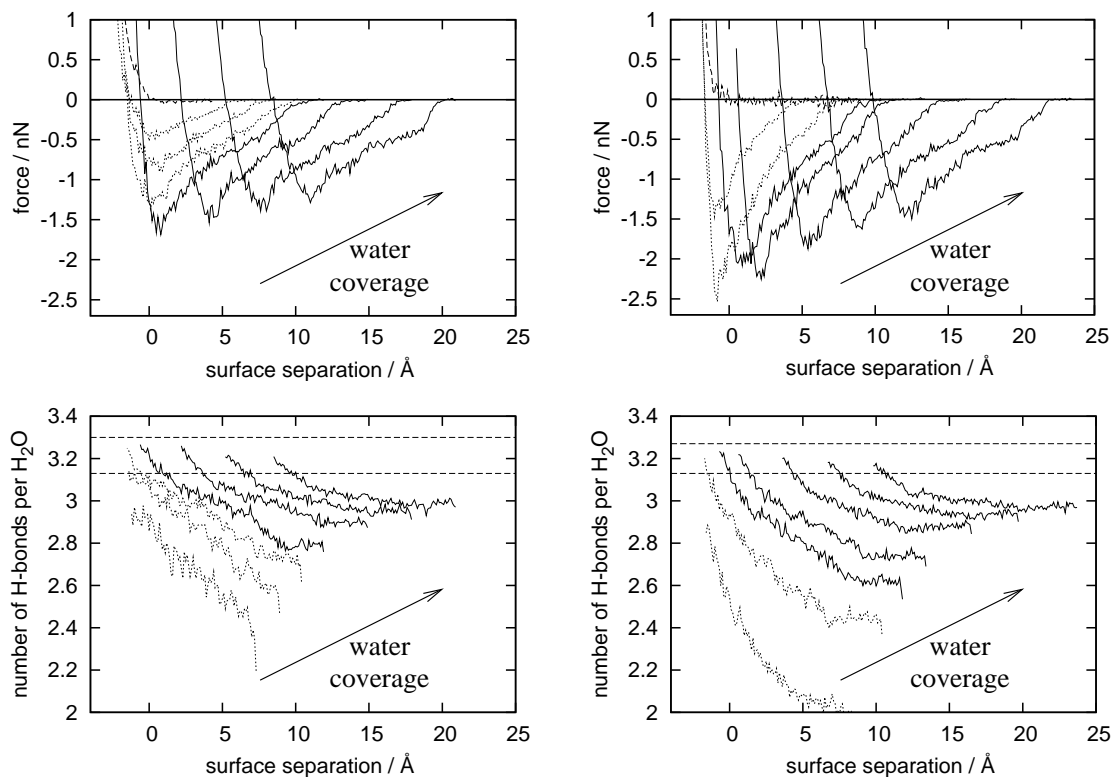
D. J. Cole et al., Figure 5



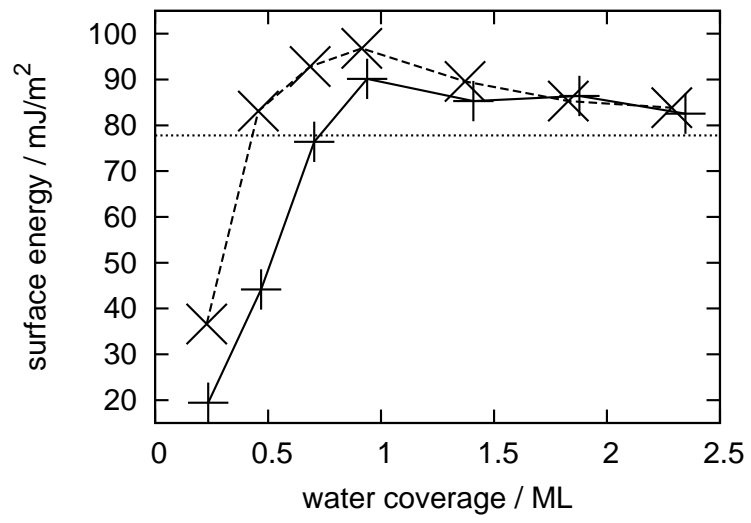
D. J. Cole et al., Figure 6



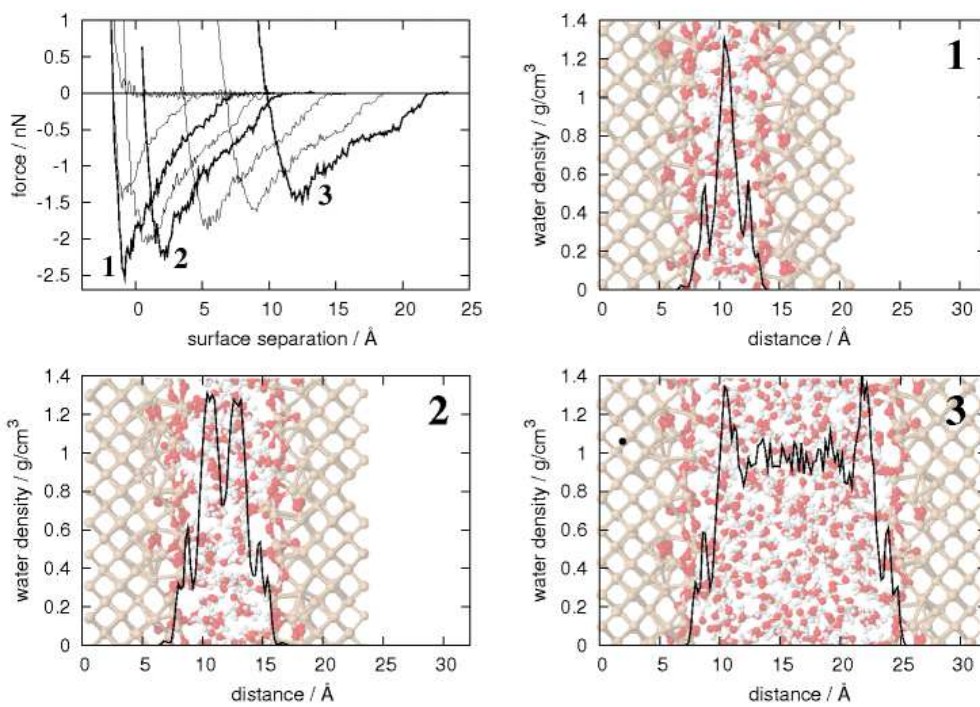
D. J. Cole et al., Figure 7



D. J. Cole et al., Figure 8



D. J. Cole et al., Figure 9



D. J. Cole et al., Figure 10